Journal of Computational Physics **151,** 790–815 (1999)
Article ID jcph.1999.6220, available online at http://www.idealibrary.com on IDEAL®

A Second-Order Godunov Method for Wave Problems in Coupled Solid–Water–Gas Systems

H. S. Tang and F. Sotiropoulos

School of Civil and Environmental Engineering, Georgia Institute of Technology, Atlanta, Georgia 30332-0355

Received March 12, 1998; revised January 13, 1999

We present a second-order Godunov method for computing unsteady, one-dimensional wave problems with fracture and cavitation in coupled solid–water–gas systems. The method employs a hydro-elasto-plastic body, the Tait equation, and the ideal gas law for solid, water, and gaseous phases, respectively, and models both fractures and cavities as vacuum zones with distinct borders. The numerical approach utilizes a Lagrangian formulation in conjunction with local solid–water–gas-vacuum Riemann problems, which have unique solutions and can be solved efficiently. The various phases are treated in a unified manner and no supplementary interface conditions are necessary for tracking material boundaries. Calculations are carried out for Riemann problems, wave propagation and reflection in a water–rock–air system, and spallation and cavitation in an explosion–steel–water–gas system. It is shown that the Godunov method has high resolution for shocks and phase interfaces, clearly resolves elastic and plastic waves, and successfully describes onset and propagation of fracture and cavitation zones.

1. INTRODUCTION

Wave problems in solid–water–gas systems with distinct phase interfaces are commonly encountered in practice, such as in water entry of a recovered body, reservoir-dam interaction during earthquakes, and spallation of steel plates caused by blast waves. In these systems each phase obeys a different equation of state (EOS) and interacts with the others in a nonlinear manner. These complexities make numerical simulation of the multiphase problems a particularly formidable task.

The conventional numerical approach for simulating such problems is based on decomposing the multiphase systems into individual phases and solving each phase separately. The coupling and interaction among phases is accounted for by supplementary conditions at phase interfaces. This approach has been successful in many applications, including problems in multiple spatial dimensions, e.g., [1, 2]. However, it does require some

0021-9991/99 $30.00

simplifications. For example, in a solid–fluid interaction problem, the computation may be limited to an elastic solid and an incompressible flow (e.g., [3]). Furthermore, certain difficulties such as non-physical oscillations may arise across phase interfaces and corrective remedies have to be adopted, e.g., [4, 5]. Additionally, in calculations of shock waves in solid phases, the standard numerical method has been to use central differencing to discretize in space the equations of motion in non-conservation form. Consequently, artificial dissipation terms need to be explicitly introduced to suppress numerical oscillations (e.g., [6]).

Godunov's method provides a novel alternative for developing numerical algorithms for multiphase systems. In recent years, Godunov-type methods were developed and successfully applied to calculate dynamic responses of solid media. Trangenstein and Colella [7] conducted an extensive study to establish a second-order Godunov scheme for computing finite deformation in isotropic elasto-plastic solids with work-hardening. Trangenstein and Pember [8] extended the scheme to the Eulerian frame of reference. Wang *et al.* [9] described another Godunov method for studying elastoplasticity of a hyperelastic material with small anisotropy. More recently, Godunov-type methods have been introduced to investigate multiphase problems. Miller and Puckett [10] designed a second-order Godunov scheme for materials in condensed phases, i.e., liquids and solids in hydrostatic limit. They employed a model based on the Mie–Gruneisen EOS and a linear Hugoniot, and their scheme is capable of handling spallation. Miller and Puckett [10] also reported that Colella *et al.* [11] proposed a Godunov method for two or more gases. Tang and Huang [12] extended the standard MUSCL scheme developed by van Leer [13] to flows of gas and water with vacuum zones. For the extension several techniques were presented to prevent the computed density from becoming smaller than its lower bound. The resulting scheme, denoted as an E-MUSCL scheme, can capture shocks, gas/water interfaces, as well as vacuum zones and takes into account water's capability to resist tensile stresses. The E-MUSCL scheme was applied to study cavitation phenomena within a water shock tube [12, 14].

The objective of this paper is to develop a second-order Godunov method for computing unsteady, one-dimensional wave problems with fracture and cavitation in coupled solid–water–gas systems, in which there are distinct interfaces between different phases. Given the existing E-MUSCL scheme [12] for coupled gas and water systems with vacuum zones, to accomplish this objective a new solid phase formulation must be developed that can be naturally incorporated into it. A major difference between responses of a solid and those of a fluid is that the former usually behaves as a shape-memory material. That is, under small applied forces it exhibits elasticity and tends to return to its original shape when the forces are removed. Under sufficiently large applied forces, on the other hand, the solid tends to become plastic and acquire a permanent deformation even after the forces are removed. Therefore, as a result of plasticity, responses of a solid cannot be uniquely determined without the knowledge of its prior history. In this paper, a solid is modeled as a hydro-elasto-plastic body—a model frequently adopted in engineering, such as high-velocity impact and explosive working, e.g., [15]. The Murnagham equation and Hooke's law are used for the hydrostatic pressure and the shear stress, respectively, in the EOS of the model. Under simple tension or simple compression, which is valid for a solid cell during small time intervals, the EOS is a single valued strain-stress curve and the equations of motion become a hyperbolic system of conservation laws. In addition, fractures within a solid are treated as vacuums. Consequently, solutions to relevant solid phase Riemann problems can be constructed and obtained by methods similar to those employed for gas–

water-vacuum Riemann problems in [12]. All these elements will be incorporated into the new solid phase scheme.

Our Godunov method handles all phases as single systems and treats different phases in a unified manner—that is, same numerical procedures are employed for all phases. The two kinds of solid–water–gas-vacuum Riemann problems involved in the proposed approach, one being a classic Riemann problem and the other being a generalized one, have unique solutions and can be solved either with a Newton iterative method or via simple algebraic formulas. Locations of material boundaries (phase interfaces, fracture borders, and cavity borders) are determined directly by solutions of local Riemann problems at grid nodes, thus eliminating the need for supplementary interface conditions. Moreover, our method is conservative and needs no explicit artificial dissipation term other than that inherent in it.

This paper is organized in seven sections. In Section 2 we present the governing equations and fracture and cavitation models. Section 3 constructs resolution of the classic Riemann problem, describes procedures to solve the problem, and discusses existence and uniqueness of its solution. Section 4 deals with the generalized Riemann problem. In Section 5, our formulation for coupled solid–water–gas systems is presented. Section 6 displays the results of computations we have made with the method to demonstrate its performance and robustness. Finally, in Section 7 we summarize the Godunov method and discuss future work. In the current paper we only give final results for water and gaseous phases. An extensive analysis about them can be found in [12].

2. GOVERNING EQUATIONS

2.1. *Equations of Motion*

In Lagrangian coordinates, the equations of motion for both an elastic-plastic solid in plane strain and an inviscid flow in one spatial dimension can be formulated in conservation form as

$$\frac{\partial U}{\partial t} + \frac{\partial F(U)}{\partial r} = 0, \tag{2.1a}$$

where

$$U = (V, u, E)^T, \tag{2.1b}$$

$$F(U) = (-u, P, uP)^T. \tag{2.1c}$$

Here, the independent variables are the time t and the mass coordinate r. $V = \rho_{ref.}/\rho$, $P = p/\rho_{ref.}$, and $E = e + u^2/2$, where $\rho_{ref.}$ is a reference density. The unknowns are ρ, the density, u, the velocity, p, the pressure in the fluid or the r-direction stress in the solid, and e, the internal energy. For convenience, we also refer to the r-direction stress as pressure in this paper. The mass coordinate r is related to the space coordinate x by

$$r = \frac{1}{\rho_{ref.}} \int_0^x \rho(t, \eta)\, d\eta. \tag{2.2}$$

All three differential equations in (2.1) will be used for a gas, whereas, due to their EOS as shown below, only the first two equations in (2.1) will be employed for either a water and a solid phase. Pressure is continuous across a material boundary, and it is zero if the interface is adjacent to a vacuum.

2.2. *Equations of State*

A solid usually exhibits behaviors much different from those of a fluid. However, it presents features of fluids under sufficiently large forces. A hydro-elasto-plastic body is a solid model that can reflect properties of fluids, while naturally and continuously describes the transition between a solid and a fluid [16]. The EOS of such a model may be written as

$$p = w(V) + \frac{4}{3}s(V_s, \tau_s, V), \tag{2.3a}$$

where $w(V)$ and $s(V_s, \tau_s, V)$ are hydrostatic pressure and shear stress, respectively, the subscript s referring to an initial state. We use the Murnagham equation for the hydrostatic pressure,

$$w(V) = \frac{m}{\beta}\left(\left(\frac{V_a}{V}\right)^{\beta} - 1\right) + p_a \tag{2.3b}$$

and the Huber–Mises criterion and Hooke's law for the shear stress,

$$s(V_s, \tau_s, V) = \begin{cases} \tau, & |\tau| < Y/2, \\ Y\,\mathrm{sign}(\tau)/2, & |\tau| \geq Y/2, \end{cases} \tag{2.3c}$$

where

$$\frac{\partial \tau}{\partial t} = -\frac{G}{V}\frac{\partial V}{\partial t}. \tag{2.3d}$$

In EOS (2.3), G, m, Y, and $\beta(\geq 1)$ are the modulus of rigidity, the bulk modulus, the yield stress, and a positive constant, respectively, and the subscript a refers to standard atmospheric conditions. $G = E/(2(1-\mu))$ and $m = E/(3(1-2\mu))$, E and μ being Young's modulus and Poisson's ratio, respectively. The EOS (2.3) corresponds to a work-hardening material, and it gives a $p - V$ relation as shown in Fig. 1. In the figure it is seen that for any state

$$w(V) - \frac{2Y}{3} \leq p \leq w(V) + \frac{2Y}{3}, \tag{2.4}$$

and lines $p = w(V) \pm 2Y/3$ correspond to plastic deformations and any path between the two lines relates to an elastic deformation. Although the EOS does not include some factors such as entropy increase, it describes a solid's elasticity and plasticity and fluid behaviors in a simple way and thus is often used.

In case of simple tension or simple compression, (2.3) can be rewritten as the $p - V$ curve

$$p = \begin{cases} w(V) + \frac{2}{3}Y, & V \leq V_2, \\ w(V) + \frac{4}{3}(G \ln \frac{V_s}{V} + \tau_s), & V_2 < V \leq V_1, \\ w(V) - \frac{2}{3}Y, & V > V_1. \end{cases} \tag{2.5a}$$

Here

$$V_1 = V_s e^{(2\tau_s + Y)/(2G)}, \tag{2.5b}$$

$$V_2 = V_s e^{(2\tau_s - Y)/(2G)}. \tag{2.5c}$$

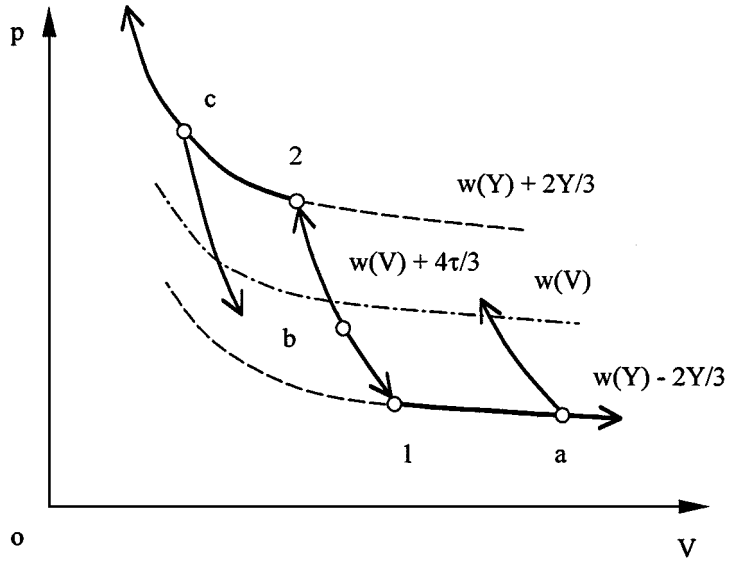

FIG. 1. The EOS (2.3): 1 and 2 respectively represent the tension and the compression yield points induced by loading.

If initial state s is at point b in Fig. 1, then the curve is $-c-2-b-1-a-$, on which p is a single valued, monotone function of V.

In fact, the above model may be an approximation to some other solid models. For instance, in case of a small deformation and $\beta = 1$, from curve (2.5a) we can derive that

$$p \approx \begin{cases} m\left(\frac{V_a}{V} - 1\right) + p_a + \frac{2}{3}Y, & V \le V_2, \\ m\left(\frac{V_a}{V} - 1\right) + p_a + \frac{4}{3}\left(G\left(\frac{V_s}{V} - 1\right) + \tau_s\right), & V_2 < V \le V_1, \\ m\left(\frac{V_a}{V} - 1\right) + p_a - \frac{2}{3}Y, & V > V_1. \end{cases} \tag{2.6}$$

In view that $V_a/V - 1$ is the r-direction strain, (2.6) defines a piecewise linear stress-strain curve, and it is actually the well-known linear elastic-perfectly plastic model. Let Y be infinity; (2.3) reduces to an elastic model.

For a water phase we use the Tait equation as its EOS

$$p = p_a k\left(\left(\frac{V_a}{V}\right)^{\alpha} - 1\right) + p_a, \tag{2.7}$$

where $k = 3045$ and $\alpha = 7.15$. Equation (2.7) is accurate enough up to a pressure of 10^9 Pa in magnitude (see [17]). For a gaseous phase we have the ideal gas law

$$p = (\gamma - 1)e\rho, \tag{2.8}$$

where γ is the ratio of specific heats.

2.3. *Fracture and Cavitation Models*

Fracture or cavitation will take place at the region where pressure drops to a critical value p_v,

$$p = p_v, \tag{2.9}$$

where the subscript v refers to fracture or cavitation conditions. Solid and water phases are capable of resisting tensile stresses while gaseous phases do not possess this capability; $p_{vep} < 0$, $p_{vw} \le 0$, and $p_{vg} = 0$, subscripts ep, w, and g standing for solid, water, and gaseous phases, respectively. In general, $p_{vg} \ge p_{vw} \ge p_{vep}$. A solid may also break owing to fatigue, and the following is the criterion due to Tuler and Butcher [18] for the event,

$$\int_0^{\delta} \left(\frac{p_f - \min(p,\, p_f)}{|p_f|} \right)^{\lambda} dt = K, \tag{2.10}$$

where p_f is the critical pressure for onset of the fatigue, δ is the time when the solid cracks, and λ and K are constants. Moreover, unlike water phases, a solid will no longer be able to support any tensile stress at the place where it once cracks in history.

In view of the above, we assume that: (1) *fracture or cavitation will take place at the region where* (2.9) *is satisfied. Also, a fracture will appear once* (2.10) *holds*. (2) p_v *takes different values at different places,*

$$p_v = \begin{cases} \phi p_{vep}, & \text{in solid,} \\ p_{vw}, & \text{in water,} \\ p_{vg}, & \text{in gas,} \\ p_{vw}, & \text{at solid–water interface,} \\ p_{vg}, & \text{at solid–gas interface,} \\ p_{vg}, & \text{at water–gas interface,} \end{cases} \tag{2.11}$$

where $\phi = 0$ *or* 1, *corresponding to the case that the solid does or does not crack in history, respectively.* (3) *Either a fracture or a cavity is regarded as a vacuum.*

The fracture and the cavitation models are similar to those employed by other authors (e.g., [15, 19]).

3. THE RIEMANN PROBLEM

3.1. *Solution of the Riemann Problem*

Consider the Riemann problem of (2.1), or the initial value problem for the system (2.1) with initial conditions given by the step function

$$U_{t=0} = \begin{cases} H_l, & r < r_0, \\ H_r, & r > r_0, \end{cases} \tag{3.1}$$

where r_0 is a constant, $H = (V, u, E)^T$, being a state of a gas, a water, a solid, or a vacuum, and the subscripts l and r denote the left and right sides of r_0, respectively.

In general, the solution to a Riemann problem for a hyperbolic system of conservation laws consists of centered waves connected by constant states. In the solution of Riemann

problems (2.1) and (3.1), the number of the centered waves depends on the difference between H_l and H_r and behaviors of the medium at either side of r_0. In addition, even if neither H_l nor H_r is a vacuum state, a vacuum will take place at r_0 after resolution of initial discontinuity (3.1) when the following condition is satisfied,

$$u_l - u_r \le \int_{\rho_l}^{\rho_v} \frac{c}{\rho}\, d\rho + \int_{\rho_r}^{\rho_v} \frac{c}{\rho}\, d\rho, \tag{3.2}$$

where $c = \sqrt{\partial p/\partial \rho}$, being the Eulerian sound speed. As shown in Subsection 3.2, (3.2) is equivalent to (2.9). Since the initial discontinuity is resolved within no time, (2.10) will not be used as a criterion for onset of a vacuum. For detailed discussions about the solution to a Riemann problem readers may refer to [20, 21, 12].

Let subscript s be l or r and an asterisk indicate resolved values beside r_0. We first consider the case that initial discontinuity (3.1) has a solid at one side of r_0. Assuming that only simple tension and compression takes place and using (2.5) and Fig. 1, we construct resolved wave systems in the solid as follows.

(1) $P^* \le P_1$. In this case, after the resolution there are two rarefactions in the solid, a leading elastic wave and trailing plastic wave. For the elastic and plastic waves one has, respectively,

$$u_1 - u_s = \pm \int_{\rho_s}^{\rho_1} \frac{c}{\rho}\, d\rho \tag{3.3a}$$

and

$$u^* - u_1 = \pm \int_{\rho_1}^{\rho^*} \frac{c}{\rho}\, d\rho. \tag{3.3b}$$

The signs $\pm$ refer to the direction of propagation of a wave, here a rarefaction, the positive and the negative signs being the right and the left, respectively. Equations (3.3) yield

$$u^* - u_s = \pm \int_{\rho_s}^{\rho^*} \frac{c}{\rho}\, d\rho. \tag{3.4}$$

(2) $P_1 < P^* \le P_s$. Now there is only one rarefaction, an elastic wave, and (3.4) still holds.

(3) $P_s < P^* \le P_2$. An elastic shock is present. Rankine–Hugoniot conditions read

$$\pm W_e(V^* - V_s) + (u^* - u_s) = 0, \tag{3.5a}$$

$$\pm W_e(u^* - u_s) - (P^* - P_s) = 0, \tag{3.5b}$$

where W_e is the Lagrangian speed of the elastic shock. It is derived form (3.5) that

$$u^* - u_s = \pm \frac{P^* - P_s}{W_e}, \tag{3.6a}$$

$$W_e = \sqrt{\frac{P^* - P_s}{V_s - V^*}}. \tag{3.6b}$$

(4) $P_2 < P^* \le P_3$. Subscript 3 refers to a point where

$$\frac{P_3 - P_2}{V_3 - V_2} = \frac{P_2 - P_s}{V_2 - V_s}. \tag{3.7}$$

At this time, there are two shocks, a leading elastic shock and a trailing plastic shock. R-H conditions for the two shocks yield

$$u^* - u_s = \pm\left(\sqrt{(P_2 - P_s)(V_s - V_2)} + \frac{P^* - P_2}{W_p}\right), \tag{3.8a}$$

$$W_p = \sqrt{\frac{P^* - P_2}{V_2 - V^*}}. \tag{3.8b}$$

Here, W_p is the Lagrangian speed of the plastic shock.

(5) $P^* > P_3$. Now, a single steady elasto-plastic shock occurs and one has

$$u^* - u_s = \pm\frac{P^* - P_s}{W_{ep}}, \tag{3.9a}$$

$$W_{ep} = \sqrt{\frac{P^* - P_s}{V_s - V^*}}, \tag{3.9b}$$

where W_{ep} is the Lagrangian speed of the elasto-plastic shock.

The discussions from (1) through (5) can be summarized as

$$u^* - u_s = \pm f_{ep}(V_s, P_s, P^*), \tag{3.10a}$$

where

$$f_{ep}(V_s, P_s, P^*) = \begin{cases} \int_{\rho_s}^{\rho^*} \frac{c}{\rho} d\rho, & P^* \le P_s, \\ \frac{P^* - P_s}{W_e}, & P_s < P^* \le P_2, \\ \sqrt{(P_2 - P_s)(V_s - V_2)} + \frac{P^* - P_2}{W_p}, & P_2 < P^* \le P_3, \\ \frac{P^* - P_s}{W_{ep}}, & P^* > P_3. \end{cases} \tag{3.10b}$$

If $\beta = 1$, it is readily seen from (2.5) or Fig. 1 that when $P^* > P_2$ the following always holds:

$$\frac{P^* - P_2}{V^* - V_2} > \frac{P_2 - P_s}{V_2 - V_s}. \tag{3.11}$$

Therefore, the above elasto-plastic shock will never occur. This case may be treated as $P_3 = +\infty$.

By similar discussions we obtain for a water phase the formula

$$u^* - u_s = \pm f_w(P_s, P^*), \tag{3.12a}$$

where

$$f_w(P_s, P^*) = \begin{cases} \frac{2V_sC_s}{\alpha-1}\left(\frac{V^*C^*}{V_sC_s} - 1\right), & P^* \le P_s, \\ \frac{P^*-P_s}{W_w}, & P^* > P_s, \end{cases} \tag{3.12b}$$

$$W_w = \sqrt{\frac{P^* - P_s}{V_s - V^*}}, \tag{3.12c}$$

and for a gaseous phase

$$u^* - u_s = \pm f_g(V_s, P_s, P^*), \tag{3.13a}$$

where

$$f_g(V_s, P_s, P^*) = \begin{cases} \frac{2V_sC_s}{\gamma-1}\left(\left(\frac{P^*}{P_s}\right)^{(\gamma-1)/2\gamma} - 1\right), & P^* \le P_s, \\ \frac{P^*-P_s}{W_g}, & P^* > P_s, \end{cases} \tag{3.13b}$$

$$W_g = C_s\sqrt{\frac{(\gamma+1)P^* + (\gamma-1)P_s}{2\gamma P_s}}. \tag{3.13c}$$

Here, W_w and W_g are the Lagrangian speed of a shock in the water and the gaseous phases, respectively, and $C \equiv \sqrt{-\partial P/\partial V} = c/V$, being the Lagrangian sound speed.

Combining (3.10), (3.12), and (3.13) we come to the conclusion that

$$u^* - u_s = \pm f(V_s, P_s, P^*), \tag{3.14a}$$

where

$$f(V_s, P_s, P^*) = \begin{cases} f_{ep}(V_s, P_s, P^*), & \text{in solid,} \\ f_w(P_s, P^*), & \text{in water,} \\ f_g(V_s, P_s, P^*). & \text{in gas,} \end{cases} \tag{3.14b}$$

and $P^* \in (P_v, +\infty)$.

When both H_l and H_r are not a vacuum state but (3.2) is satisfied, or, when either H_l or H_r is a vacuum state, (3.14) gives

$$\begin{aligned} P^* &= 0, \\ u^* &= \pm f(V_s, P_s, 0) + u_s. \end{aligned} \tag{3.15}$$

In case of (3.15), u^* and P^* are determined explicitly, whereas, iteration is needed in solving (3.14a). We eliminate u^* in (3.14a) and then have

$$f(V_l, P_l, P^*) + f(V_r, P_r, P^*) - (u_l - u_r) = 0. \tag{3.16}$$

If we define

$$F(P) \equiv f(V_l, P_l, P) + f(V_r, P_r, P) - (u_l - u_r), \tag{3.17}$$

Eq. (3.16) can be solved by the Newton iterative method

$$P^{(n+1)} = P^{(n)} - \left(\frac{F(P)}{dF(P)/dP} \right)^{(n)}, \tag{3.18a}$$

where

$$P^{(0)} = P_v \tag{3.18b}$$

and the superscript (n) refers to the nth iteration.

If $P < P_s$, a numerical quadrature is necessary for calculating $f_{ep}(V_s, P_s, P)$. We chose the Simpson formula for the quadrature, and the truncation error of the formula is of order $O(1/m^4)$, m being the total number of nodes in the quadrature. In solving (2.14a), to achieve the full accuracy of the formula, $O(P^{(N)} - P^*)$ should be no larger than $O(1/m^4)$, N being the total number of the iteration.

Once P^* and u^* are obtained, the value of V^* is available. In a solid phase, when $V_2 < V^* \le V_1$, one may also use a Newton iterative method to solve (2.5a); it is easy to verify that the method converges if its initial value is set as V_2. Otherwise, one can obtain V^* from (2.5a) explicitly. In a water phase, V^* is given by (2.7). In a gas, V^* is available from the R-H condition

$$\pm W_g(V^* - V_s) + (u^* - u_s) = 0 \tag{3.19a}$$

in case that a shock is present at side s, or, the isoentropic relation

$$\frac{p^*}{\rho^{*\gamma}} = \frac{p_s}{\rho_s{}^{\gamma}} \tag{3.19b}$$

in case that a rarefaction is present at side s.

3.2. *Existence and Uniqueness of the Solution to the Riemann Problem and Convergence of its Solver*

LEMMA 3.1. *$f(V_s, P_s, P)$ is a continuous and monotonically increasing function of P, and its first and second derivatives are positive and negative, respectively.*

Proof. First, we consider $f_{ep}(V_s, P_s, P)$. Since $f_{ep}(V_s, P_s, P)$ is continuous within $(-\infty, P_s]$, $(P_s, P_2]$, $(P_2, P_3]$, and $(P_3, +\infty)$ and in view of

$$\lim_{P \to P_s \pm 0} f_{ep}(V_s, P_s, P) = f_{ep}(V_s, P_s, P_s), \tag{3.20a}$$

$$\lim_{P \to P_2 \pm 0} f_{ep}(V_s, P_s, P) = f_{ep}(V_s, P_s, P_2), \tag{3.20b}$$

$$\lim_{P \to P_3 \pm 0} f_{ep}(V_s, P_s, P) = f_{ep}(V_s, P_s, P_3), \tag{3.20c}$$

it is known that $f_{ep}(V_s, P_s, P)$ changes continuously with P. Differentiating (3.10b), one obtains

$$\frac{df_{ep}(V_s, P_s, P)}{dP} = \begin{cases} \frac{1}{C}, & P \le P_s, \\ \frac{1}{2}\left(\frac{1}{W_e} + \frac{W_e}{C^2}\right), & P_s < P \le P_2, \\ \frac{1}{2}\left(\frac{1}{W_p} + \frac{W_p}{C^2}\right), & P_2 < P \le P_3, \\ \frac{1}{2}\left(\frac{1}{W_{ep}} + \frac{W_{ep}}{C^2}\right), & P > P_3. \end{cases} \tag{3.21}$$

Furthermore, by a long but straightforward calculation, one has

$$\frac{d^2 f_{ep}(V_s, P_s, P)}{dP^2} = \begin{cases} -\frac{\beta+1}{2C^3V}, & P \le P_1, \\ -\frac{1}{2C^5}\left(\frac{m(\beta+1)}{\rho_{ref.}V^2} + \frac{4G}{3\rho_{ref.}V^2}\right), & P_1 < P \le P_s, \\ -\frac{1}{2C^4}\left(\frac{\left(W_e^2 - C^2\right)^2}{2W_e^3(V_s - V)} + \frac{m(\beta+1)W_e}{\rho_{ref.}C^2V^2} + \frac{4GW_e}{3\rho_{ref.}C^2V^2}\right), & P_s < P \le P_2, \\ -\frac{1}{2C^4}\left(\frac{\left(W_p^2 - C^2\right)^2}{2W_p^3(V_s - V)} + \frac{(\beta+1)W_p}{V}\right), & P_2 < P \le P_3, \\ -\frac{1}{2C^4}\left(\frac{\left(W_{ep}^2 - C^2\right)^2}{2W_{ep}^3(V_s - V)} + \frac{(\beta+1)W_{ep}}{V}\right), & P > P_3. \end{cases} \tag{3.22}$$

It is then seen that the first and second derivatives of $f_{ep}(V_s, P_s, P)$ are positive and negative, respectively.

Second, by similar discussions we can conclude that Lemma 3.1 is also true for both $f_w(P_s, P)$ and $f_g(V_s, P_s, P)$. For details refer to [12]. This completes the proof of Lemma 3.1. ■

Assertion 3.1. Criterion (3.2) is equivalent to criterion (2.9).

Actually, we can interpret criterion (2.9) as when P^* drops to its lowest possible value P_v

$$u_+^* > u_-^*, \tag{3.23}$$

where the subscripts $-$ and $+$ stand for the left and the right sides of r_0, respectively. Then from (3.14a) we know that (2.9) holds true if and only if (3.2) is satisfied. Furthermore, we have

THEOREM 3.1. (1) *The solution, as constructed in Subsection* 3.1, *to the Riemann problem for* (2.1) *with* (3.1) *exists uniquely.* (2) *The Newton iterative method* (3.18) *converges to the solution if it has no vacuum state.*

Proof. (1) When either H_l or H_r is a vacuum state, the problem has a unique solution P^*, u^*, and V^* simply given by (3.15), (2.5), (2.7), and (3.19).

When neither H_l nor H_r is a vacuum state, there are two possible cases. The first is that (3.2) is satisfied. In this case, a vacuum takes place, and P^*, u^*, and V^* are also determined uniquely by (3.15), (2.5), (2.7), and (3.19).

The second case is that (3.2) does not hold, that is, no vacuum occurs after the resolution and P^* is given by (3.16). Now we have

$$u_l - u_r > \int_{\rho_l}^{\rho_v} \frac{c}{\rho} d\rho + \int_{\rho_r}^{\rho_v} \frac{c}{\rho}\, d\rho, \tag{3.24}$$

namely

$$F(P_v) < 0. \tag{3.25}$$

The definition of $F(P)$ yields

$$F(+\infty) = +\infty > 0. \tag{3.26}$$

Besides, it is known from Lemma 3.1 that $F(P)$ is a monotonically increasing function of P. As a result, $F(P)$ passes the point of zero once and only once, i.e., (3.16) has a unique solution $P^* \in (P_v, +\infty)$. In view of (3.14a), (2.5), (2.7), and (3.19), the existence and uniqueness of P^* guarantees the existence and uniqueness of u^* and V^*. Therefore, the Riemann problem has a unique solution.

(2) Consider an interval (P_v, M), where M is a constant sufficiently large such that $F(M) > 0$ and $P^* \in (P_v, M)$. We conclude from (3.25), (3.26), and Lemma 3.1 that (1) $F(P_v)F(M) < 0$, (2) $dF(P)/dP \neq 0$, (3) $dF^2(P)/dP^2 < 0$, and (4) $(F(P) \cdot dF^2(P)/dP^2)_{P=P_v} > 0$. It can be proven that iteration (3.18) tends to its fixed point (cf. [22]):

$$\lim_{n\to\infty} P^{(n)} = P^*. \tag{3.27}$$

This completes the proof of the theorem. ■

4. THE GENERALIZED RIEMANN PROBLEM

For accuracy enhancement in the proposed Godunov method, we consider the initial value problem for (2.1) with the initial data

$$U_{t=0} = \begin{cases} Q_l(r), & r < r_0, \\ Q_r(r), & r > r_0, \end{cases} \tag{4.1a}$$

where $Q(r) = (V(r), u(r), E(r))^T$, each component of $Q(r)$ being a linear function of r, and

$$\lim_{r\to r_0-0} Q_l(r) = H_l, \qquad \lim_{r\to r_0+0} Q_r(r) = H_r. \tag{4.1b}$$

The initial value problem for (2.1) with (4.1) is regarded as a generalized Riemann problem of the classic Riemann problem for (2.1) with (3.1). We make a hypothesis similar to that in [23]: at $t = 0+$ the generalized Riemann problem has a solution with the same wave structure as that of its associate classic Riemann problem and, consequently, (3.14) or (3.15) holds true. Under this assumption we derive the formulas for time derivatives $(\partial u/\partial t)^*$ and $(\partial P/\partial t)^*$ as follows.

First, consider the case that the solution of the generalized Riemann problem has no vacuum state. Differentiating (3.14a) and using (2.1), one can obtain expressions for $(\partial u/\partial t)^*$ and $(\partial P/\partial t)^*$. For example, in a solid phase within which $P_v < P^* \leq P_s$, differentiating (3.14a) yields

$$\frac{D}{Dt}(u^* - u_s) = \pm\frac{D}{Dt}\int_{\rho_s}^{\rho^*} \frac{c}{\rho} d\rho. \tag{4.2}$$

Letting $(D/Dt)^* = \partial/\partial t \pm C^*\partial/\partial r$ and $(D/Dt)_s = \partial/\partial t \pm C_s\partial/\partial r$ in (4.2) and employing (2.1) give the expression

$$\left(\frac{\partial u}{\partial t}\right)^* \pm \left(-\frac{1}{C^*}\right)\left(\frac{\partial P}{\partial t}\right)^* = \pm C_s\left(\frac{\partial u}{\partial r}\right)_s - \left(\frac{\partial P}{\partial r}\right)_s. \tag{4.3}$$

Similarly, the expressions in the other cases can be obtained. Two of these expressions, one corresponding to the right side of r_0 and the other to the left side of r_0, comprise the following linear algebraic system for the time derivatives,

$$\begin{pmatrix} a_{11} & -a_{12} \\ a_{21} & a_{22} \end{pmatrix} \begin{pmatrix} \left(\frac{\partial u}{\partial t}\right)^* \\ \left(\frac{\partial P}{\partial t}\right)^* \end{pmatrix} = \begin{pmatrix} b_1\left(\frac{\partial u}{\partial r}\right)_s & -b_2\left(\frac{\partial P}{\partial r}\right)_s \\ -b_1\left(\frac{\partial u}{\partial r}\right)_s & -b_2\left(\frac{\partial P}{\partial r}\right)_s \end{pmatrix}, \tag{4.4a}$$

where for a solid phase

$$a_{11}, a_{21} = \begin{cases} 1, & P^* \le P_s, \\ \frac{W_e^2}{2C^{*2}} + \frac{3}{2}, & P_s < P^* \le P_2, \\ \frac{W_p^2}{2C^{*2}} + \frac{3}{2}, & P_2 < P^* \le P_3, \\ \frac{W_{ep}^2}{2C^{*2}} + \frac{3}{2}, & P^* > P_3, \end{cases} \tag{4.4b}$$

$$a_{12}, a_{22} = \begin{cases} \frac{1}{C^*}, & P^* \le P_s, \\ \frac{3W_e}{2C^{*2}} + \frac{1}{2W_e}, & P_s < P^* \le P_2, \\ \frac{3W_p}{2C^{*2}} + \frac{1}{2W_p}, & P_2 < P^* \le P_3, \\ \frac{3W_{ep}}{2C^{*2}} + \frac{1}{2W_{ep}}, & P^* > P_3, \end{cases} \tag{4.4c}$$

$$b_1 = \begin{cases} C_s, & P^* \le P_s, \\ \frac{3W_e}{2} + \frac{C_s^2}{2W_e}, & P_s < P^* \le P_3, \\ \frac{3W_{ep}}{2} + \frac{C_s^2}{2W_{ep}}, & P^* > P_3, \end{cases} \tag{4.4d}$$

$$b_2 = \begin{cases} 1, & P^* \le P_s, \\ \frac{W_e^2}{2C_s^2} + \frac{3}{2}, & P_s < P^* \le P_3, \\ \frac{W_{ep}^2}{2C_s^2} + \frac{3}{2}, & P^* > P_3, \end{cases} \tag{4.4e}$$

for a water phase

$$a_{11}, a_{21} = \begin{cases} \frac{W_{wr}^2}{C^*} + W_{wr}, & P^* \le P_s, \\ \frac{W_w^3}{2C^{*2}} + \frac{3W_w}{2}, & P^* > P_s, \end{cases} \tag{4.4f}$$

$$a_{12}, a_{22} = \begin{cases} \frac{W_{wr}^2}{C_s^2} + \frac{W_{wr}}{C^*}, & P^* \le P_s, \\ \frac{3{W_w}^2}{2C^{*2}} + \frac{1}{2}, & P^* > P_s, \end{cases} \tag{4.4g}$$

$$b_1 = \begin{cases} W_{wr}^2 + C_s W_{wr}, & P^* \le P_s, \\ \frac{3W_w^2}{2} + \frac{C_s^2}{2}, & P^* > P_s, \end{cases} \tag{4.4h}$$

$$b_2 = \begin{cases} \frac{W_{wr}^2}{C_s} + W_{wr}, & P^* \le P_s, \\ \frac{W_w^3}{2C_s^2} + \frac{3W_w}{2}, & P^* > P_s, \end{cases} \tag{4.4i}$$

$$W_{wr} = \frac{(\alpha - 1)(P^* - P_s)}{2(V^*C^* - V_sC_s)}, \tag{4.4j}$$

and for a gaseous phase

$$a_{11}, a_{21} = \begin{cases} \frac{W_{gr}^2}{C^*} + W_{gr}, & P^* \le P_s, \\ \frac{(\gamma+1)(V^*-V_s)W_g}{4V_s} + 2W_g, & P^* > P_s, \end{cases} \tag{4.4k}$$

$$a_{12}, a_{22} = \begin{cases} \frac{W_{gr}^2}{C_s^2} + \frac{W_{gr}}{C^*}, & P^* \le P_s, \\ \frac{W_g^2}{C^{*2}} + \frac{(\gamma+1)(V^*-V_s)}{4V_s} + 1, & P^* > P_s, \end{cases} \tag{4.4l}$$

$$b_1 = \begin{cases} -\left(1 - \frac{W_{gr}}{C^*}\right)\frac{C_s^2 P^*}{P_s} + W_{gr}^2 + \frac{(\gamma+1)(P^*-P_s)}{2V_s} + C_s^2, & P^* \le P_s, \\ -\frac{(V^*-V_s)W_g^2}{2V_s} + W_g^2 - \frac{(\gamma-1)(V^*-V_s)C_s^2}{4V_s} + C_s^2, & P^* > P_s, \end{cases} \tag{4.4m}$$

$$b_2 = \begin{cases} -\left(1 - \frac{W_{gr}}{C^*}\right)\frac{P^* W_{gr}}{P_s} + \frac{(\gamma+1)(P^*-P_s)W_{gr}}{2V_s C_s^2} + 2W_{gr}, & P^* \le P_s, \\ -\frac{(V^*-V_s)W_g^3}{2V_s C_s^2} - \frac{(\gamma-1)(V^*-V_s)W_g}{4V_s} + 2W_g, & P^* > P_s, \end{cases} \tag{4.4n}$$

$$W_{gr} = \frac{(\gamma-1)P_s^{(\gamma-1)/2\gamma}(P^*-P_s)}{2V_s C_s\left(P^{*(\gamma-1)/2\gamma} - P_s^{(\gamma-1)/2\gamma}\right)}. \tag{4.4o}$$

It is easy to verify that in the solid, the water, and the gas ($\gamma \le 3$) $a_{km} > 0$ ($k, m = 1, 2$). Consequently,

$$DET(a_{km}) = a_{11}a_{22} + a_{12}a_{21} > 0. \tag{4.5}$$

According to linear algebra, we have the following conclusion.

Assertion 4.1. Under the restriction of $\gamma \le 3$, the solution of (4.4a) exists uniquely.

Second, we consider the case that the solution has a vacuum state. At this time,

$$\left(\frac{\partial P}{\partial t}\right)^* = 0, \tag{4.6}$$

and (4.4a) gives rise to

$$\left(\frac{\partial u}{\partial t}\right)^* = \frac{1}{a_{11}}\left(\pm b_1\left(\frac{\partial u}{\partial r}\right)_s - b_2\left(\frac{\partial P}{\partial r}\right)_s\right). \tag{4.7}$$

5. THE SECOND-ORDER GODUNOV METHOD

Construct a grid in such a way that each material boundary will be right at a grid node. Integrating system (2.1) over $[t^n, t^{n+1}] \times [r_i, r_{i+1}]$, using the Green formula, and omitting third and higher order terms, we have the following Lagrangian formulations in conservation form,

$$\bar{V}_{i+1/2}^{n+1} = \bar{V}_{i+1/2}^{n} + \lambda_{i+1/2}^{n}\left(\langle u\rangle_{(i+1)-}^{n} - \langle u\rangle_{i+}^{n}\right). \tag{5.1a}$$

$$\bar{u}_{i+1/2}^{n+1} = \bar{u}_{i+1/2}^{n} - \lambda_{i+1/2}^{n}\left(\langle P\rangle_{(i+1)-}^{n} - \langle P\rangle_{i+}^{n}\right), \tag{5.1b}$$

$$\bar{E}_{i+1/2}^{n+1} = \bar{E}_{i+1/2}^{n} - \lambda_{i+1/2}^{n}\left(\langle u\rangle_{(i+1)-}^{n}\langle P\rangle_{(i+1)-}^{n} - \langle u\rangle_{i+}^{n}\langle P\rangle_{i+}^{n}\right), \tag{5.1c}$$

where

$$\langle u\rangle = u^* + \frac{1}{2}\left(\frac{\partial u}{\partial t}\right)^* \Delta t, \tag{5.1d}$$

$$\langle P\rangle = P^* + \frac{1}{2}\left(\frac{\partial P}{\partial t}\right)^* \Delta t, \tag{5.1e}$$

$\lambda^n_{i+1/2} = \Delta^n t/\Delta_{i+1/2} r$, $\Delta^n t = t^{n+1} - t^n$, the time step, and $\Delta_{i+1/2} r = r_{i+1} - r_i$, the grid spacing. The grid does not necessarily have a uniform spacing. To determine the RHS of (5.1d) and (5.1e), we need to solve local Riemann problems and local generalized Riemann problems, as formulated in Sections 3 and 4, respectively, at node r_i. The states beside the initial discontinuity of the problems are given by

$$\bar{R}^n_{i-1/2} + \frac{\Delta^n_{i-1/2} R^*}{\Delta_{i-1/2} r}(r - r_{i-1/2}), \qquad r < r_i, \tag{5.2a}$$

and

$$\bar{R}^n_{i+1/2} + \frac{\Delta^n_{i+1/2} R^*}{\Delta_{i+1/2} r}(r - r_{i+1/2}), \qquad r > r_i, \tag{5.2b}$$

or, (5.2a) or (5.2c) and a vacuum state. Here $r_{i+1/2} = (r_i + r_{i+1})/2$ and $\Delta^n_{i+1/2} R^*$ is a cell slope,

$$\Delta^n_{i+1/2} R^* = \langle R\rangle^{n-1}_{(i+1)-} - \langle R\rangle^{n-1}_{i+}, \tag{5.2c}$$

where R refers to V, u, and P. In a solid phase V^* and P^* are related to each other by (2.5), in which the initial state can be $\bar{V}^{n+1}_{i\pm1/2}$ and $\bar{P}^n_{i\pm1/2}$. If the discontinuity is comprised by (5.2a) and (5.2b), i.e., initially there is no vacuum state at node r_i, a new vacuum may take place there either for the sake of

$$u^n_{i-} - u^n_{i+} \le \int_{V_v}^{V_{i-}} C\, dV + \int_{V_v}^{V_{i+}} C\, dV, \tag{5.3a}$$

which is derived form (3.2), or, due to

$$\Sigma_n \left(\frac{P_f - \min\left(\left(\bar{P}^n_{i-1/2} + \bar{P}^n_{i+1/2}\right)/2,\, P_f\right)}{|P_f|}\right)^{\lambda} \Delta^n t = K, \tag{5.3b}$$

which is derived from (2.10).

Once $\bar{V}_{i+1/2}$, $\bar{u}_{i+1/2}$, and $\bar{E}_{i+1/2}$ are updated using (5.1), $\bar{P}_{i+1/2}$ can be computed as follows. Assume that pressure in each cell of the solid increases or decreases monotonically during the time interval (t^n, t^{n+1}). Then (2.3) gives rise to

$$\bar{\tau}^{n+1}_{i+1/2} = \bar{\tau}^n_{i+1/2} - G \ln \frac{\bar{V}^{n+1}_{i+1/2}}{V^n_{i+1/2}}, \tag{5.4a}$$

and

$$\bar{P}^{n+1}_{i+1/2} = \begin{cases} \frac{1}{\rho_{ref.}}\left(w\left(\bar{V}^{n+1}_{i+1/2}\right) + \frac{2}{3}Y\right), & \bar{V}^{n+1}_{i+1/2} \le V^{n+1}_{i+1/2,2}, \\ \frac{1}{\rho_{ref.}}\left(w\left(\bar{V}^{n+1}_{i+1/2}\right) + \frac{4}{3}\tau^{n+1}_{i+1/2}\right), & V^{n+1}_{i+1/2,2} < \bar{V}^{n+1}_{i+1/2} \le V^{n+1}_{i+1/2,1}, \\ \frac{1}{\rho_{ref.}}\left(w\left(\bar{V}^{n+1}_{i+1/2}\right) - \frac{2}{3}Y\right), & V^{n+1}_{i+1/2} > \bar{V}^{n+1}_{i+1/2,1}, \end{cases} \tag{5.4b}$$

where

$$V_{i+1/2,1}^{n+1} = \bar{V}_{i+1/2}^{n} e^{\left(2\bar{\tau}_{i+1/2}^{n}+Y\right)/(2G)}, \tag{5.4c}$$

$$V_{i+1/2,2}^{n+1} = \bar{V}_{i+1/2}^{n} e^{\left(2\bar{\tau}_{i+1/2}^{n}-Y\right)/(2G)}. \tag{5.4d}$$

From (2.7) and (2.8) we respectively obtain for a cell of water the sufficiently accurate formula

$$\bar{P}_{i+1/2}^{n+1} = \frac{p_a}{\rho_{ref.}}\left(k\left(\left(\frac{\rho_{ref.}}{\rho_a \bar{V}_{i+1/2}^{n+1}}\right)^{\alpha} - 1\right) + 1\right) \tag{5.5}$$

and for a cell of gas

$$\bar{P}_{i+1/2}^{n+1} = \frac{\gamma - 1}{\bar{V}_{i+1/2}^{n+1}}\left(\bar{E}_{i+1/2}^{n+1} - \frac{\bar{u}_{i+1/2}^{n+1\ 2}}{2}\right). \tag{5.6}$$

Each cell's location in the Euler frame of reference is tracked by evaluating the positions of its two ends via the formula

$$x_{i\pm}^{n+1} = x_{i\pm}^{n} + \langle u \rangle_{i\pm}^{n} \Delta^n t. \tag{5.7}$$

We assume that a vacuum may and only may appear between two slabs, i.e., right at a grid node. A vacuum zone is bounded by its two ends and its position can also be tracked by (5.7). In calculations, if a vacuum is very small (when $|x_{i+} - x_{i-}| \le \epsilon$, ϵ being positive and sufficiently small), it will be ignored.

Equations (5.1)–(5.7) are the method we propose for solid–water–gas systems. The method deals with different phases in unified procedures, and it only employs (5.7), which is necessary for tracking interior nodes, but no other extra conditions in tracking material boundaries. Since it uses the same basic techniques as the standard MUSCL scheme due to van Leer [13] and the previous E-MUSCL scheme [12] and contains both of them as its special cases, formulation (5.1)–(5.7) may still be referred to as an E-MUSCL scheme, a further extended version of the standard MUSCL scheme. If all cell slopes are set equal to zero, the current E-MUSCL scheme will reduces to a first-order Godunov scheme.

In computations two algorithms are necessary. The first is a monotonicity algorithm proposed by van Leer [13] to suppress numerical oscillations:

$$\Delta_{i+1/2}^{n} R^* = \begin{cases} \min\left(2\left|\Delta_i^n \bar{R}\right|, \left|\Delta_{i+1/2}^{n} R^*\right|, 2\left|\Delta_{i+1}^{n} \bar{R}\right|\right) \operatorname{sgn}\Delta_{i+1/2}^{n} R^*, \\ \qquad \operatorname{sgn}\Delta_i^n \bar{R} = \operatorname{sgn}\Delta_{i+1}^{n} \bar{R} = \operatorname{sgn}\Delta_{i+1/2}^{n} R^*, \\ 0, \qquad \text{otherwise.} \end{cases} \tag{5.8}$$

Here, $\Delta_i^n \bar{R} = \bar{R}_{i+1/2}^{n} - \bar{R}_{i-1/2}^{n}$. The second is an algorithm of lower bound of density to prevent the computed density from becoming smaller than its lower bound ρ_v [12]:

$$\Delta_{i+1/2}^{n} u^* = \min\left(\Delta_{i+1/2}^{n} u^*, \bar{V}_{i+1/2}^{n}\left(1 - \frac{\bar{V}_{i+1/2}^{n}}{V_v}\right)\frac{\Delta_{i+1/2} r}{\Delta^{n-1} t}\right). \tag{5.9}$$

Both (5.8) and (5.9) are limiters over cell slopes and they act as a kind of numerical viscosity.

Some restrictions on the time step are also needed. For the sake of stability, no waves issuing from one end of a slab are allowed to interact with those from the other end,

$$\Delta^n t \le \frac{\mathrm{CFL}\Delta_{i+1/2} r}{2\max\left(\left|W^n_{i+}\right|, \left|W^n_{(i+1)-}\right|\right)}, \tag{5.10}$$

where W_i is the speed of either a shock wave or a rarefaction's front and $\mathrm{CFL} \le 1$. When $\Delta^n_{i+1/2} u^* < 0$, zone-tangling (the left end of a slab moves across its right end or vice versa) is not permitted:

$$\Delta^n t \le -\frac{x^n_{(i+1)-} - x^n_{i+}}{\Delta^n_{i+1/2} u^*}. \tag{5.11}$$

At last, as a vacuum exists at node r_i and $\langle u\rangle^n_{i-} > \langle u\rangle^n_{i+}$, slab overlapping ($x_{i+} - x_{i-} < 0$) should be avoided:

$$\Delta^n t \le \frac{x^n_{i+} - x^n_{i-}}{\langle u\rangle^n_{i-} - \langle u\rangle^n_{i+}}. \tag{5.12}$$

In summary, the present formulation consists of the following major steps:

(i) Compute tension and compression yield values according to (5.4c) and (5.4d).

(ii) Mark the grid nodes where vacuums have already occurred and utilize criterion (5.3) to see if new vacuums will take place.

(iii) Use (5.2), (5.8), and (5.9) to set initial discontinuities for local Riemann problems at grid nodes.

(iv) Find solutions of the Riemann problems; obtain values of $V^*_{i\pm}$, $u^*_{i\pm}$, and P^* via (3.18), (3.14), (3.15), (2.5), (2.7), and (3.19) and calculate $(\partial u/\partial t)^*_{i\pm}$ and $(\partial P/\partial t)^*_i$ via (4.4), (4.6), and (4.7).

(v) Determine the time step with the aid of (5.10)–(5.12).

(vi) Update slab averages $\bar{V}_{i+1/2}$, $\bar{u}_{i+1/2}$, $\bar{E}_{i+1/2}$, $\bar{\tau}_{i+1/2}$, and $\bar{P}_{i+1/2}$ by (5.1) and (5.4)–(5.6), and use (5.7) to track locations of cells, phase interfaces, and vacuum zones.

6. NUMERICAL EXAMPLES

6.1. *Riemann Problems*

The following three Riemann problems are calculated to validate the ability of the present method to deal with different phases and resolve waves and vacuum zones:

$$\text{(I)}\begin{cases} x<0\text{(steel)}: \rho = 8046.83\,\mathrm{kg/m^3},\ u = -1000\,\mathrm{m/s},\ p = 8\times 10^9\,\mathrm{Pa}, \\ x>0\text{(steel)}: \rho = 7755.74\,\mathrm{kg/m^3},\ u = 1000\,\mathrm{m/s},\ p = -1.9\times 10^9\,\mathrm{Pa}, \end{cases} \tag{6.1}$$

$$\text{(II)}\begin{cases} x<0\text{(steel)}: \rho = 7800.06\,\mathrm{kg/m^3},\ u = 300\,\mathrm{m/s},\ p = 2.5\times 10^6\,\mathrm{Pa}, \\ x>0\text{(water)}: u = -300\,\mathrm{m/s},\ p = 2.5\times 10^9\,\mathrm{Pa}, \end{cases} \tag{6.2}$$

$$\text{(III)}\begin{cases} x<0\text{(steel)}: \rho = 7800\,\mathrm{kg/m^3},\ u = 0\,\mathrm{m/s},\ p = 1.01325\times 10^5\,\mathrm{Pa}, \\ x>0\text{(gas)}: \rho = 50\,\mathrm{kg/m^3},\ u = -500\,\mathrm{m/s},\ p = 10^9\,\mathrm{Pa},\ \gamma = 1.4. \end{cases} \tag{6.3}$$

TABLE I
Parameters for the Steel

Property	Value	Dimension
ρ_a	7800	kg/m^3
m	2.225×10^{11}	Pa
β	3.7	
G	8.53×10^{10}	Pa
Y	9.79×10^{8}	Pa
p_v	-2×10^{10}	Pa
p_f	-1.9292×10^{9}	Pa
λ	1.33	
K	3.35×10^{-6}	s

Properties of the steel are those employed by Chu *et al*. [15] and shown in Table I. In problem (I), after resolution of the initial discontinuity, two rarefactions propagate to the left, an elastic shock travels to the right, and a vacuum takes place between the rarefactions and the shock. The faster rarefaction is an elastic precursor, and the slower one is a plastic wave. After resolution of initial discontinuity (II), an elastic shock (a precursor) and a plastic shock move left in the solid, and a shock propagates right in the water. In problem (III), an elastic shock in the solid and a shock in the gas propagate to the left and the right, respectively.

The numerical solutions and the corresponding exact solutions for the three problems are displayed in Figs. 2–4. Comparing the numerical solutions with the exact ones, we see that our scheme correctly resolves all the waves and the vacuum zone. It captures shocks with

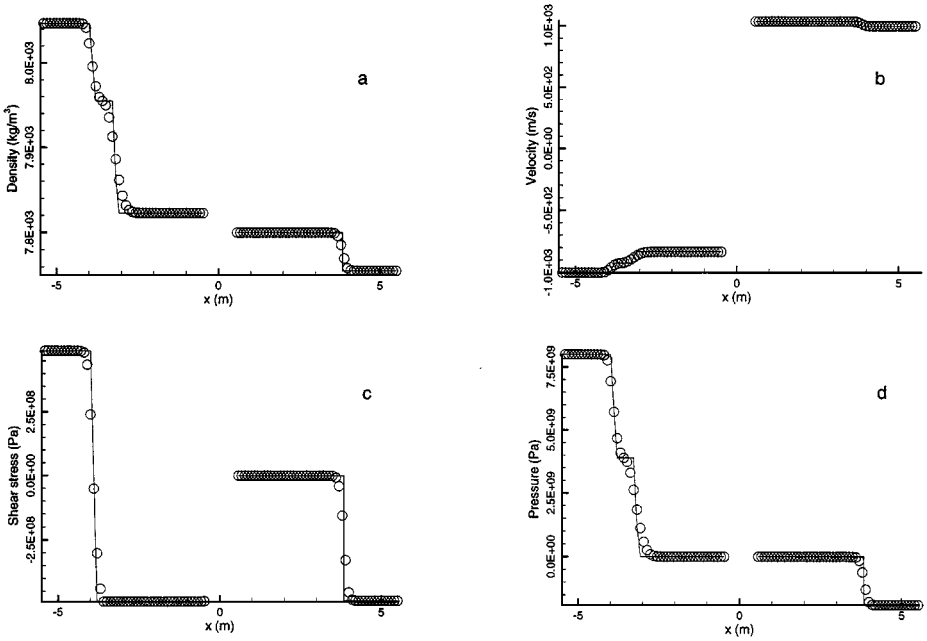

FIG. 2. Riemann problem (I). Solid lines, exact solutions; circles, numerical solutions. Cell number = 100, CFL = 1, and $t = 5.07 \times 10^{-4}$ s.

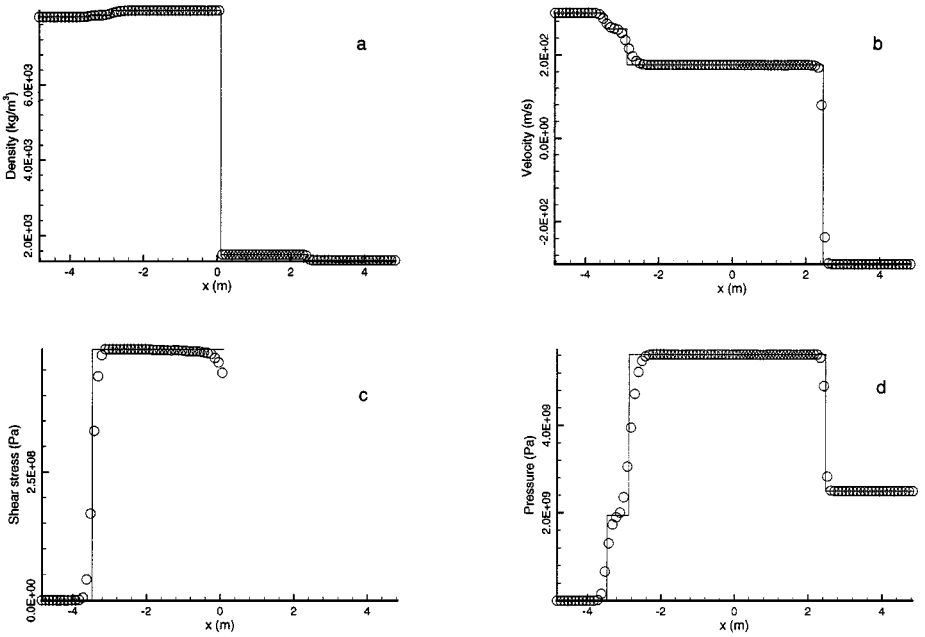

FIG. 3. Riemann problem (II). Solid lines, exact solutions; circles, numerical solutions. Cell number = 50 (steel) × 50 (water), CFL = 1, and $t = 5.46 \times 10^{-4}$ s.

narrow transition regions and essentially without oscillations, and its resolution for elastic and plastic shocks is similar to that of other second-order Godunov methods (e.g., [7]).

To illustrate that our method has second-order accuracy, we employ a first-order Godunov scheme, constructed by setting all slab slopes equal to zero, to compute the same three

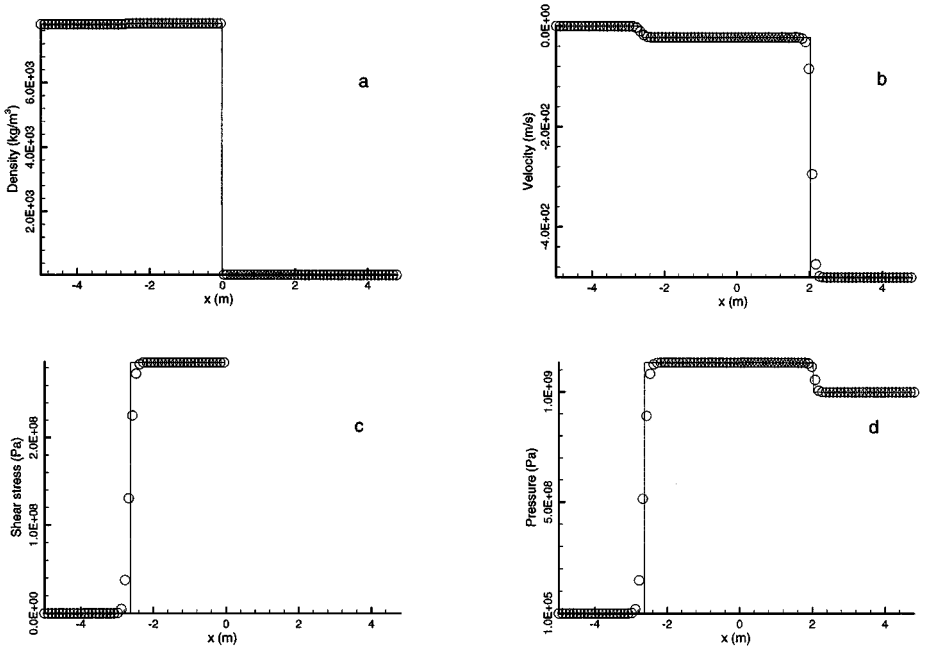

FIG. 4. Riemann problem (III). Solid lines, exact solutions; circles, numerical solutions. Cell number = 50 (steel) × 50 (gas), CFL = 1, and $t = 4.04 \times 10^{-4}$ s.

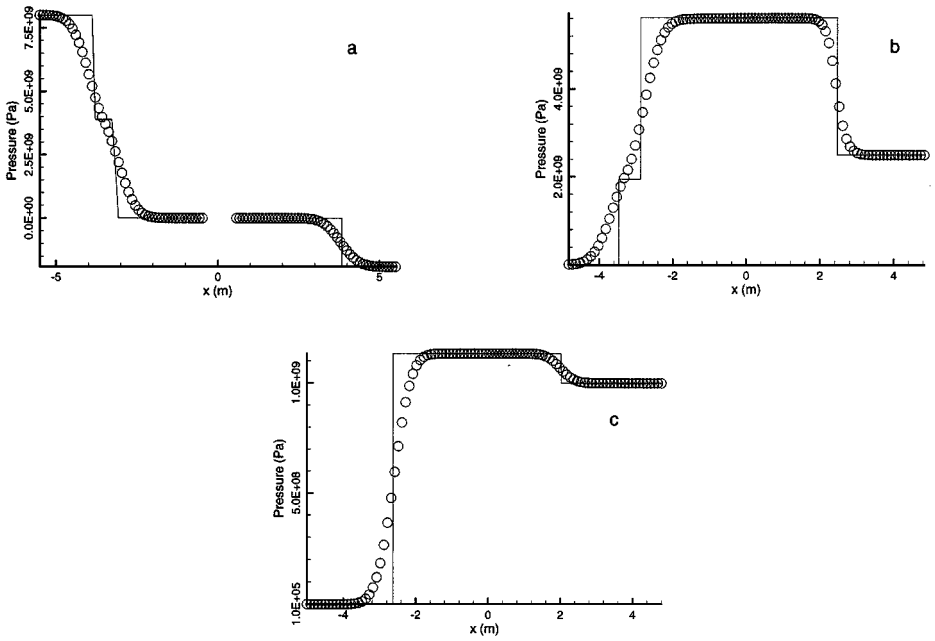

FIG. 5. Calculations using the first-order Godunov scheme. All relevant parameters are the same as those in Figs. 2, 3, and 4. Solid lines, exact solutions; circles, numerical solutions. (a) Riemann problem (I). (b) Riemann problem (II). (c) Riemann problem (III).

Riemann problems. The computed pressures are given in Fig. 5. Obviously, our method yields solutions far more accurate than those obtained by the first-order scheme. Actually, at this mesh size the first-order method fails almost entirely to resolve the elastic and plastic waves. Finally, the results of mesh refinement tests for the second-order scheme are shown in Fig. 6. It is seen that spatial resolution of the scheme improves as the mesh size decreases.

6.2. *Wave Propagation and Reflection*

Figure 7 shows the schematic of a system made up of a body of water, a rock wall, and air. In the water a shock propagates right, strikes the wall, and then induces some waves. The initial distributions are given in Table II. Under multi-dimensional stresses, rocks usually exhibit elasticity and plasticity. We use $p - V$ curve (2.5) with $\beta = 1$, or elastic-perfectly plastic model (2.6), for the rock and derive its properties displayed in Table III from relevant data given in [24].

TABLE II
Initial Distributions in the Water–Rock–Air System

		$x < -0.5$ m (water)	-0.5 m $< x < 0$ m (water)	0 m $< x <$ 1 m (rock)	$x >$ 1 m (air)
ρ	kg/m^3			2300	1.25
u	m/s	18.8852	0	0	0
p	Pa	28877500	101325	101325	101325

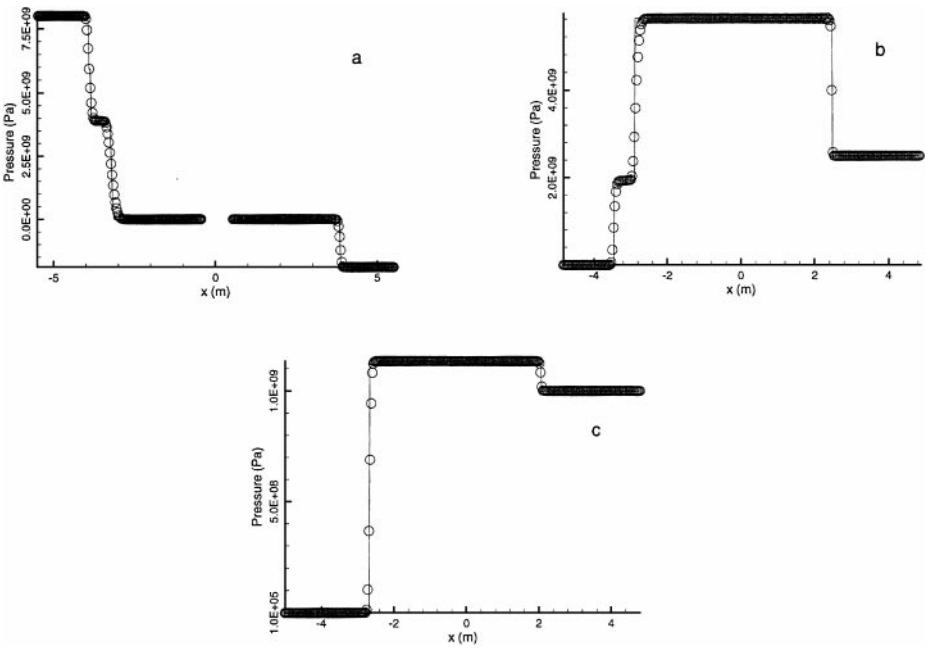

FIG. 6. Mesh refinement test. All relevant parameters are the same as those in Figs. 2, 3, and 4, except mesh size. Solid lines, exact solutions; circles, numerical solutions. (a) Riemann problem (I). Cell number = 300. (b) Riemann problem (II). Cell number = 150 (steel) × 150 (water). (c) Riemann problem (III). Cell number = 150 (steel) × 150 (gas).

As shown in Figs. 8a and 8b, initially the shock in the water moves to the right. Subsequently, the shock hits the rock, and two shocks moving right, a leading elastic and a trailing plastic wave, are generated in the rock (Figs. 8c and 8d). Finally, the two shocks reflect at the rock/air interface, and another shock moving right is produced in the air (Figs. 8e and 8f). The calculation has resolved a triple-wave structure in the rock, which is a result of interaction among different waves (see Fig. 8f). It can be seen in Fig. 8 that across the phase interfaces the numerical results exhibit no spurious oscillations reported by some authors (e.g., [5]).

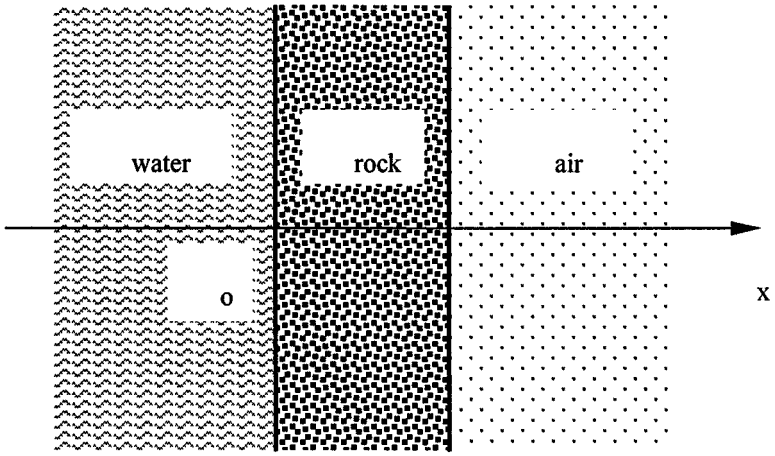

FIG. 7. Schematic representation of the water–rock–air system.

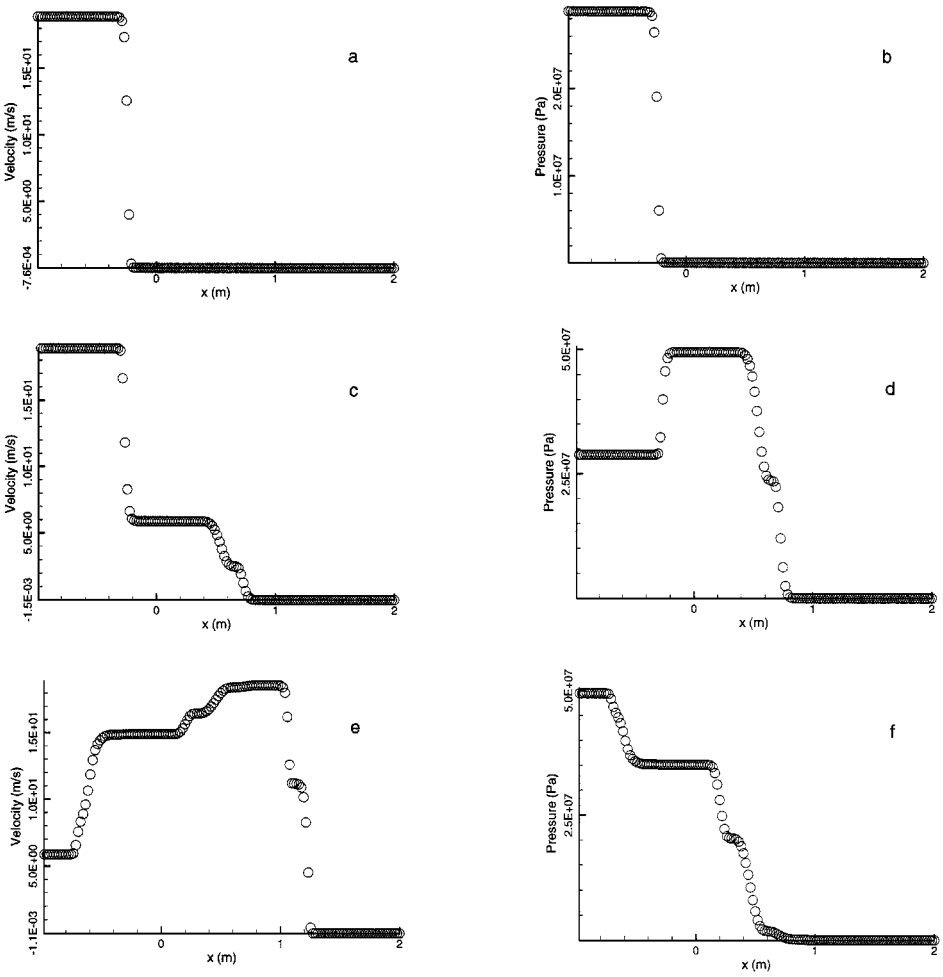

FIG. 8. Numerical results for the wave propagation and reflection. Cell number = 50 (water) × 50 (rock) × 50 (air). CFL = 1. (a), (b) $t = 1.68 \times 10^{-4}$ s. (c), (d) $t = 4.97 \times 10^{-4}$ s. (e), (f) $t = 1.25 \times 10^{-3}$ s.

6.3. *Spallation and Cavitation Induced by Explosion*

In Fig. 9, a steel plate is placed on a layer of dynamite, above the plate there is a body of water, and above the water there exists a compressed gas, whose top is constrained by a rigid wall. After the dynamite is ignited, a blast propagates upwards and generates waves into the system. In the computation, the gravity is ignored, the pressure on the lower surface of the dynamite is approximated as zero, and the explosion product is treated as a perfect gas. The

TABLE III
Parameters for the Rock

Property	Value	Dimension
ρ_a	2300	kg/m^3
m	2.528×10^{10}	Pa
G	1.002×10^{10}	Pa
Y	1.2159×10^{7}	Pa

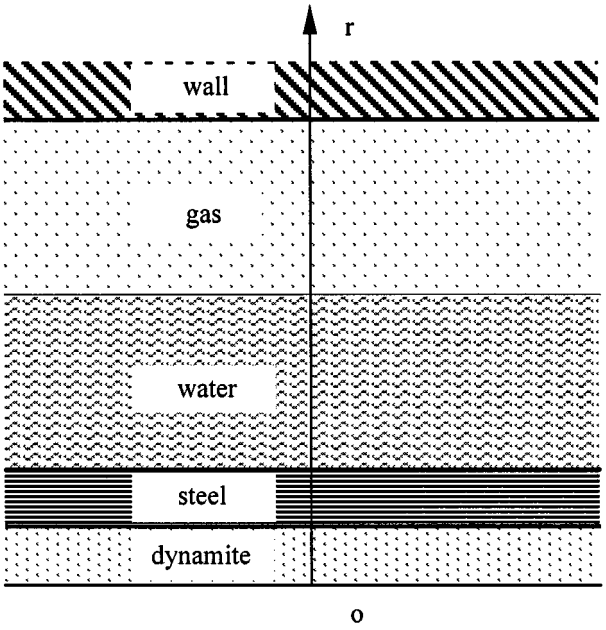

FIG. 9. Schematic description of the explosion-steel–water–gas system.

computation begins as the blast reaches the plate, and the initial and boundary conditions are shown in Table IV. In the table $\rho(r)$, $u(r)$, and $p(r)$ are determined analytically by the dynamite density and the blast speed (see [25]), which are 1600 kg/m^3 and 7667 m/s in the computation, respectively. Again, we use properties given in Table I for the steel plate.

Due to the action of the blast, a shock followed by rarefactions propagates upwards in the plate. Our method gives a sharp profile for the shock (Fig. 10a), which is a plastic wave (its elastic precursor is too weak to be observed). After the shock reflects at the plate/water interface, downwards-moving rarefactions are created at the upper end of the plate, and an upwards-moving shock is generated in the water. The downwards- and upwards-moving rarefactions interact with each other, causing tension in the plate. Then, the plate spalls because of fatigue and the spallation zones spread downwards from a neighbor of its upper surface (Fig. 10b). Once the shock in the water reaches the water/gas interface, the gas is compressed (Fig. 10c). Similarly, at a later time, the water cavitates and the cavitation zones propagate downwards from the water/gas interface. The process of spallation and cavitation

TABLE IV

Initial and Boundary Conditions in the Explosion-Steel–Water–Gas System

r m ($\rho_{ref.} = 1$ kg/m^3)	ρ kg/m^3	u m/s	p Pa
0 (vacuum)			0
0–160 (explosion product, $\gamma = 1.4$)	$\rho(r)$	$u(r)$	$p(r)$
160–1720 (steel)	7800.01	0	506625
1720–2720 (water $p_v = 0$)		0	506625
2720–2726.125 (gas, $\gamma = 1.4$)	6.125	0	506625
2726.125 (rigid wall)		0	

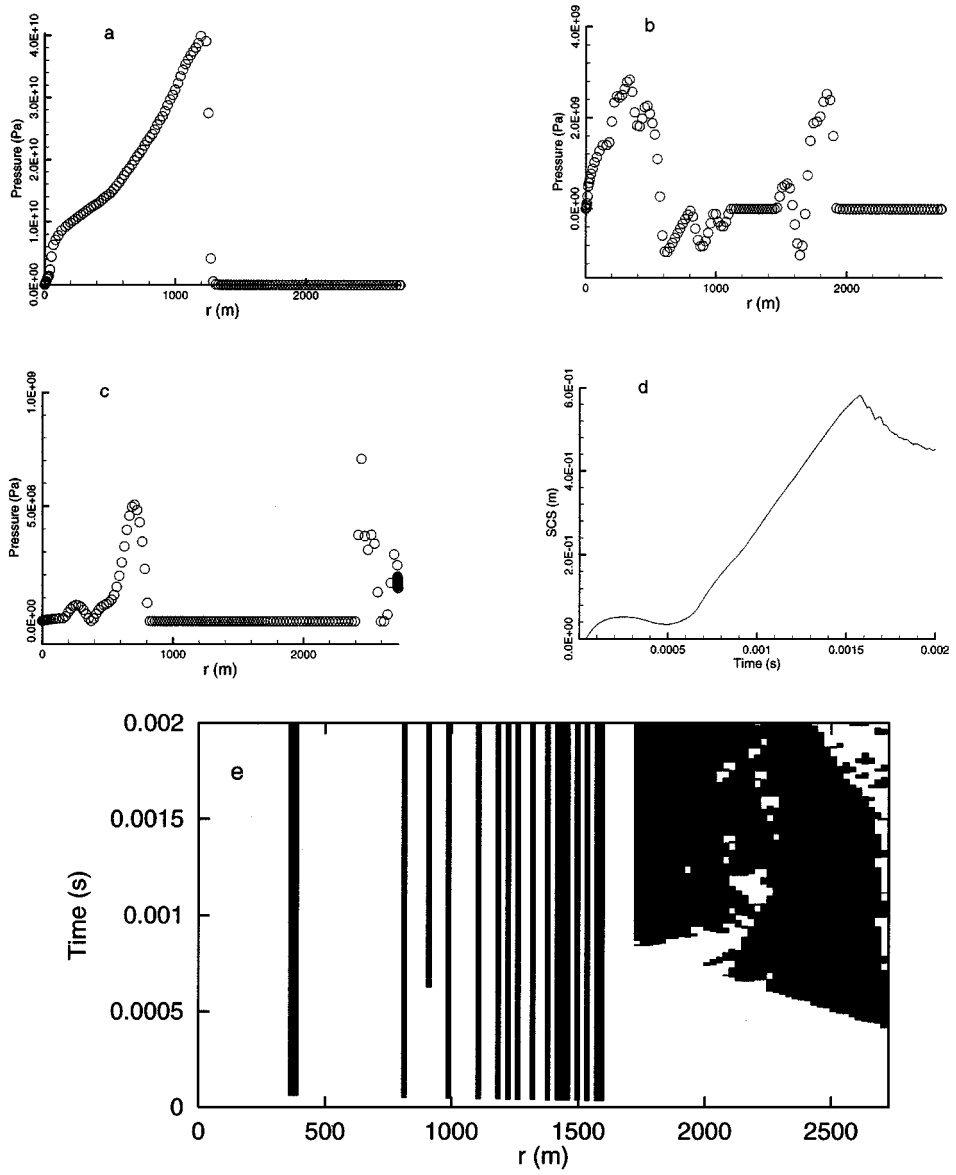

FIG. 10. Numerical results for the spallation and cavitation. Cell number = 30 (explosion product) × 80 (steel plate) × 40 (water) × 40 (gas). CFL = 1. (a) A shock propagates upwards in the plate, $t = 2.12 \times 10^{-5}$ s. (b) A shock propagates upwards in the water, $t = 7.93 \times 10^{-4}$ s. (c) The gas is compressed, $t = 2.00 \times 10^{-3}$ s. (d) Strength of the spallation and cavitation. $SCS = \sum_i (x_{i+} - x_{i-})$. (e) Spallation and cavitation zones. The plate spalls in the left shadow of stripes, while the water cavitates in the right shadow regions.

can be seen from the computed results given in Figs. 10d and 10e. Calculations on finer meshes yield a process of spallation and cavitation similar to that shown in Figs. 10d and 10e.

7. CONCLUDING REMARKS

We have developed a second-order accurate Godunov method for computing unsteady, one-dimensional wave problems in coupled solid–water–gas systems. The method, referred

to as an E-MUSCL scheme, is a sequel to Tang and Huang's scheme [12], which is based on van Leer's MUSCL scheme [13]. The method has three key features: (i) it employs the hydro-elasto-plastic body, the Tait equation, and the ideal gas law to model solid, water, and gaseous phases, respectively; (ii) it utilizes the solutions of local solid–water–gas-vacuum Riemann problems; and (iii) it uses the Lagrangian frame of reference to facilitate the tracking of material boundaries. A series of numerical experiments were carried out to validate and test the accuracy and robustness of the method and underscore its ability to capture shock waves and phase interfaces with high resolution, clearly resolve elastic and plastic waves, and successfully describe onset and propagation of fracture and cavitation zones.

The proposed approach treats all phases using the same numerical procedures and eliminates the need for extra techniques to track material boundaries. This attribute is important as it considerably simplifies programming. Furthermore, in the class of wave system we have constructed, the classic solid–water–gas-vacuum Riemann problem has a unique solution and can be solved efficiently either by a Newton iterative method or by explicit formulas. These properties of the Riemann problem compensate for its complexity and enhance the efficiency of the entire methodology. It is also necessary to point out that our method can be applied to systems consisting of multiple regions occupied by phases of the same material but with different parameters—provided, of course, that behaviors of each such material can be described by one of the assumed EOS (e.g., two gases with different values of γ or two solids with different sets of m and β). Therefore, the present method could be very useful in studying various engineering problems such as those involving laminated composite plates.

The present Godunov methodology is strictly applicable to one-dimensional systems. Its extension, with the three features mentioned above, to multiple spatial dimensions is far from being trivial. A critical issue that needs to be addressed, in that context, is the algorithm for tracking material boundaries in a multi-dimensional space, particularly, prediction of crack paths in solids and shapes of cavitation zones in water. However, we anticipate that such an extension is feasible, at least for some relatively simple cases, with the aid of rezoning and front tracking techniques. Moreover, it is readily seen that in the EOS (2.3), p or stress is a piecewise convex function of V or strain. In fact, an alternative for the solid phase scheme of the Godunov methodology may be developed if another solid phase EOS is used that defines stress as a piecewise linear or convex function of strain. Finally, it should be pointed out that the efficiency and overall simplicity of the proposed approach can be further enhanced, without significantly compromising its accuracy, by replacing the exact solvers with approximate ones for the solid–water–gas-vacuum Riemann problems.

ACKNOWLEDGMENTS

This work was supported in part by the Natural Science Foundation of China and the Aeronautic Science Foundation of China when the first author worked in the School of Space Technology, Beijing University of Aeronautics and Astronautics, Beijing. Partial support was also provided by the School of Civil and Environmental Engineering, Georgia Institute of Technology, Atlanta.

REFERENCES

1. C. Rajakumar and A. Ali, Boundary element-finite element coupled eigenanalysis of fluid-structure systems, *Int. J. Numer. Methods Eng.* **39**, 1625 (1996).

2. Sh. U. Galiev, Influence of cavitation upon anomalous behavior of a plate/liquid/underwater explosion system, *Int. J. Impact Eng.* **19**, 345 (1997).
3. S. S. Babu and S. K. Bhattacharyya, Finite element analysis of fluid-structure interaction effect on liquid retaining structures due to sloshing, *Comput. Structure* **59**, 1165 (1996).
4. R. D. Richtmyer and K. W. Morton, *Difference Methods for Initial-Value Problems*, 2nd ed. (Interscience, New York, 1967).
5. S. Karni, Hybird multifluid algorithms, *SIAM J. Sci. Comput.* **17**, 1019 (1996).
6. M. L. Wilkins, Calculation of elastic-plastic flow, *Methods Comp. Phys.* **3**, 211 (1964).
7. J. Trangenstein and P. Colella, A higher-order Godunov method for modeling finite deformation in elastic-plastic solids, *Comm. Pure Appl. Math.* **44**, 41 (1991).
8. J. Trangenstein and R. B. Pember, Numerical algorithms for strong discontinuities in elasticplastic solids, *J. Comput. Phys.* **103**, 63 (1992).
9. F. Wang, J. G. Glimm, J. W. Grove, and B. J. Plohr, A conservative Eulerian numerical scheme for elstoplasticity and application to plate impact problems, *Impact Comput. Sci. Eng.* **5**, 285 (1993).
10. G. H. Miller and E. G. Puckett, A high-order Godunov method for multiple condensed phases, *J. Comput. Phys.* **128**, 134 (1996).
11. P. Colella, H. M. Glaz, and R. E. Ferguson, Multigrid algorithms for Eulerian finite difference methods, manuscript, 1996.
12. H. S. Tang and D. Huang, A second-order accurate capturing scheme for 1D inviscid flows of gas and water with vacuum zones, *J. Comput. Phys.* **128**, 301 (1996).
13. B. van Leer, Towards the ultimate conservative difference scheme. V. A second-order sequel to Godunov's method, *J. Comput. Phys.* **32**, 101 (1979).
14. H. S. Tang, Numerical study of cavitation phenomenon in water shock tube, *J. Hydrodynamics A* **12**, 175 (1997). [In Chinese]
15. C. H. Chu, Y. C. Li, and X. J. Wang, Numerical analysis of steel plate's spallation due to explosion, *Appl. Math. Mech.* **2**, 353 (1981). [In Chinese]
16. G. L. Trigg, *Encyclopedia of Applied Physics* (VCH Publishers, New York, 1997), Vol. 18.
17. Yu. S. Yiakovlev, *Hydrodynamics of Explosion* (State Press of Ship Industry, Leningrad, 1961). [In Russian]
18. F. R. Tuler and M. B. Butcher, A criterion for the time dependence of dynamic fracture, *Int. J. Fra. Mech.* **4**, 431 (1968).
19. R. A. Wentell, H. D. Scott, and R. P. Chapman, Cavitation due to shock pulses reflected from the sea surface, *J. Acoust. Soc. Am.* **46**, 789 (1969).
20. P. Lax, Hyperbolic systems of conservation laws, II, *Comm. Pure Appl. Math.* **10**, 537 (1957).
21. T. P. Liu and J. A. Smoller, On the vacuum state for the isentropic gas dynamics equations, *Adv. Appl. Math.* **1**, 345 (1980).
22. Z. H. Chao, Y. D. Zhang, and R. X. Li, *Computing Matrixes and Solving Equations* (High Education Press, Beijing, 1979). [In Chinese]
23. M. Ben-Artzi and J. Falcovitz, A second-order Godunov-type scheme for compressible fluid dynamics, *J. Comput. Phys.* **55**, 1 (1984).
24. J. Q. Li and S. Z. Ma, *Explosion Dynamics* (Science Press, Beijing, 1992). [In Chinese]
25. Y. L. Zhou, *One Dimensional Unsteady Fluid Dynamics* (Science Press, Beijing, 1990). [In Chinese]